Along-strike segmentation of the South China Sea margin imposed by inherited pre-rift basement structures

Fang Zhao[a], Tiago M. Alves[b], Shaohong Xia[a,*], Wei Li [a], Lei Wang[c], Lijun Mi[d], Shiguo Wu[e], Jinghe Cao[a], Chaoyan Fan[a]

[a] CAS Key Laboratory of Marginal Sea Geology, South China Sea Institute of Oceanology, Chinese Academy of Sciences, Guangzhou 510301, China

[b] 3D Seismic Lab. School of Earth and Ocean Sciences, Cardiff University, Main Building, Park Place, Cardiff, CF10 3AT, United Kingdom

[c] College of Underwater Acoustic Engineering, Harbin Engineering University, Harbin 150001, China

[d] CNOOC Nanhai East Petroleum Bureau, Shenzhen, Guangdong 518054, China

[e] Institute of Deep-Sea Science and Engineering, Chinese Academy of Sciences, Sanya 572000, China

*shxia@scsio.ac.cn (Shaohong Xia)

Abstract

Multibeam bathymetric, seismic and borehole data are used to investigate a large-scale strike-slip structure, the Baiyun-Liwan Fault Zone, in the northern South China Sea. This fault zone comprises NW- to NE-striking faults and negative flower structures that were generated by oblique extensional displacement. Notably, the interpreted data reveals that the Baiyun-Liwan Fault Zone was active during the Cenozoic,

recording intense magmatism, and accommodating significant intraplate deformation during progressive continental rifting and ocean spreading. It bounds two distinct crustal segments and played a significant role in segmenting the northern margin of the South China Sea. The geometry of faults and strata within the Baiyun-Liwan Fault Zone also controlled local sediment routing and depocentre evolution during the Cenozoic. As basement and syn-rift structures change markedly across the Baiyun-Liwan Fault Zone, we propose this structure to be inherited from a lithospheric-scale fault zone separating the Mesozoic arc from forearc-related terrains. We therefore stress the importance of pre-existing structures in the development of rifted margins, with the example provided by the Baiyun-Liwan Fault Zone having profound implications for palaeogeographic reconstructions in the South China Sea. At present, the Baiyun-Liwan Fault Zone is incised by the Pearl River Canyon and eroded by recurrent submarine landslides, forming a major area of sediment bypass towards the abyssal plain.

Keywords: South China Sea; structural inheritance; faults; magmatism; continental rifting; margin segmentation.

1. Introduction

Rifted continental margins are formed when continental lithosphere is extended, thinned, fragmented and broken apart, eventually leading to the formation of oceanic crust (Piqué and Laville, 1996; Tommasi and Vauchez, 2001; Manatschal, 2004; Peron-Pinvidic et al., 2007; Franke et al., 2013; Petersen and Schiffer, 2016). Inherited structures in continental lithosphere, such as suture zones and young orogenic belts, tend to form crustal weaknesses that play an important role in controlling the location and duration of extension, the

regional thermal structure, and the structural and depositional styles of rifted margins (Dunbar and Sawyer, 1989; Ring, 1994; Morley, 2010; Pereira and Alves, 2013; Philippon et al., 2015; Festa et al., 2019). In fact, field observations complemented by numerical and analogue models show that the nature, extent and orientation of pre-existing weakness zones in basement units are able to influence continental rifting and the post-rift evolution of continental margins, with deformation being localised in these same zones (Jackson et al., 1982; van Wijk, 2005; Corti et al., 2008; Morley, 2010; Philippon et al., 2015). Furthermore, inherited crustal structures are capable of focusing later tectonic reactivation, seismicity and strain well after continental breakup is achieved (Corti et al., 2008; Pereira and Alves, 2013).

Evidence from geological and geophysical data has shown that diachronous rifting and continental breakup dominated the Cenozoic evolution of the South China Sea (Taylor and Hayes, 1983; Ru and Pigott, 1986; Briais et al., 1993; Franke, 2013; Savva et al., 2014; Li et al., 2014; Zhao et al., 2016; Yang et al., 2018). As a result of this diachronous evolution, crustal-stretching, faulting, magmatic and subsidence histories in the South China Sea vary significantly across distinct crustal segments. Previous studies have proposed the existence of distinct tectonic terrains of a Mesozoic (pre-rift) subduction zone below the syn-rift basins of the northern South China Sea (Zhou et al., 2008; Yan et al., 2014; Wan et al., 2017; Shao et al., 2018; Li et al., 2018) (Figs. 1-3). A long pre-Cenozoic history of tectonism created pre-existing crustal heterogeneities with varied orientations, which suggestively controlled the Cenozoic crustal architecture along and across this latter continental margin (Franke, 2013; Savva et al., 2014; Yan et al., 2014; Sun et al., 2016; Shao et al., 2018; Li et al., 2018). Based on the latter postulate, this paper uses multibeam bathymetric, multi-channel (2D) seismic reflection, and borehole data from the Pearl River Mouth Basin to investigate a prominent fault zone in the northern South China Sea, named herein as Baiyun-Liwan Fault Zone, or BLFZ (Fig. 4). It is proposed that this (so far) unknown lithospheric-scale structure accommodated intraplate strain

during the evolution of the northern South China Sea. Hence, this paper addresses the following research questions:

a) In what way(s) the geometry and sedimentary infill of the BLFZ differ from other parts of the northern South China Sea?

b) What was the kinematic evolution of the BLFZ in the context of continental rifting and breakup?

c) Does the BLFZ coincide with a structural boundary inherited from the pre-rift basement of the South China Sea?

d) What relationship exists between the depositional styles of the BLFZ and major tectonic events recorded in the northern South China Sea?

2. Geological setting

2.1 General evolution of the South China Sea

The area that is now the South China Sea was strongly deformed in the Jurassic by subduction of the Palaeo-Pacific Plate below the Eurasian Plate (Taylor and Hayes, 1983; Zhou et al., 2008; Li et al., 2018). Plate subduction formed lithospheric-scale structures that imposed local controls on the thermal state of the lithosphere during Cenozoic continental rifting (Buck, 1991; Zhou et al., 2008; Manatschal et al., 2015; Sun et al., 2016; Shao et al., 2018). An example of such controls are the several high-positive magnetic anomaly trends, likely associated with Mesozoic magmatic activity, that extend southwards from the Pearl River Mouth Basin towards the Zhongsha and Xisha Islands (Zhou et al., 2008; Li et al., 2018) (Fig. 1). Petrological

data from arc-like granites, intermediate rocks and agglomerates of rock fragments associated with lava flows, suggest that the magnetic-anomaly trends originated from a Late Mesozoic volcanic arc (Li et al., 2018). In parallel, folded and thrusted Mesozoic strata, chiefly comprising Upper Jurassic to Lower Cretaceous marine units, are recognised on borehole and seismic data from Taiwan to the Chaoshan Depression and Dongsha High, indicating that tectonic accretion and compression occurred in front of the volcanic arc (Shao et al., 2007; Yan et al., 2014; Wan et al., 2017; Li et al., 2018; Shao et al., 2018) (Fig. 1d). This Late Mesozoic volcanic arc is segmented, with its northeast part crossing the central Pearl River Mouth Basin and its southwest part being close to the Northwest Sub-basin (Yan et al., 2014; Wan et al., 2017; Li et al., 2018) (Figs. 1 and 3). Hence, its location has been recognised as an important factor controlling the *loci* of continental breakup in the South China Sea, with resulting breakup regions coinciding with the volcanic front/forearc in the northeast and with the arc *per se* in the southwest (Li et al., 2018).

The South China Sea recorded multiphased continental rifting from early Eocene to late Oligocene, ultimately resulting in the formation of distinct oceanic basins (Ru and Pigott, 1986; Franke et al., 2013; Savva et al., 2014; Sun et al., 2016) (Figs. 1 and 2). Specifically in the northern South China Sea, Cenozoic extension was diachronous and records early rifting in the west Taiwan region and the central part of Pearl River Mouth Basin during the Late Paleocene. Rifting was initiated later in the Middle Eocene around the southern Pearl River Mouth and Qiongdongnan Basins (Franke et al., 2013; Savva et al., 2014; Sun et al., 2016; Yang et al., 2018) (Fig. 2).

Seafloor spreading occurred in two main tectonic pulses across the South China Sea. A regional unconformity dated as ~33 Ma at IODP Site U1435 represents the earliest regional seafloor spreading in the northern South China Sea, being accompanied an important change in regional deposition style (Li et al., 2014; Zhao et al., 2016). A second unconformity, dated as ~23.8 Ma at ODP Site 1148, records the onset of

seafloor spreading in the Southwest Sub-basin (Wang et al., 2000, Li et al., 2014, Zhao et al., 2016). The age of this unconformity fits well with a breakup-related hiatus at 22–23 Ma in the Qiongdongnan Basin (Zhou et al., 1995). After the end of seafloor spreading, subduction of the South China Sea beneath the Philippine Sea Plate shifted to a wide region along the Manila Trench, accompanying the collision between the Luzon arc and the South China Sea margin (Figs. 1 and 2). This event resulted in widespread tectonic inversion in the northern South China Sea, and promoted intense regional uplift, igneous activity, fault reactivation and erosion in the study area since the Late Miocene (McIntosh et al., 2013; Wu et al., 2014).

2.2 Regional geology

The Cenozoic geodynamic history of the Pearl River Mouth Basin can be divided into three phases: (1) a continental rifting phase initiated in the Paleogene; (2) a breakup phase recording widespread faulting and subsidence during the Early Oligocene–Early Miocene (Zhao et al., 2016), and (3) a drift phase occurring after the Middle Miocene (Fig. 2).

The study area comprises two main physiographic features, the Baiyun and Liwan Sags, comprising one of the most complex areas of the northern South China Sea (Figs. 3 and 4). The Baiyun Sag, striking NE-SW, is situated in the upper part of the continental slope, whereas the Liwan Sag follows the continent-ocean transition on the lower continental slope and rise (Figs. 3 and 4). These two sedimentary basins are separated by a structural high (Figs. 4 and 5). Geophysical and geochemical data suggest that the Baiyun and Liwan Sags are located among three distinct Mesozoic crustal segments bounded by Mesozoic arcs to the north and west, and by the Mesozoic forearc zone to the east (Yan et al., 2014; Li et al., 2018) (Fig. 3a). To the south,

129 the limit of the Liwan Sag corresponds to a series of prominent ridges marking the boundary between
130 continental and oceanic crust in physiographic terms (Fig. 4a).

131 Following rifting and seafloor spreading, extreme crustal thinning and accelerated subsidence became
132 widespread in the Baiyun and Liwan Sags (Hu et al., 2009; Xie et al., 2014). After the Early Miocene, the
133 Pearl River became the dominant drainage system into the northern South China Sea (Ding et al., 2013) (Fig.
134 3a).

135

136 *2.3 Variations in crustal segmentation along the northern South China Sea*

137

138 The crustal and lithospheric structures of the northern South China Sea have been significantly studied
139 in the past decade after the acquisition of large amounts of multi-channel seismic (MCS), ocean bottom
140 seismograph (OBS), sediment cores, magnetic and geochemical data (Nissen et al., 1995; Yan et al., 2001;
141 Wang et al., 2006; Wei et al., 2011; Wu et al., 2012; Yan et al., 2014; Savva et al., 2014; Li et al., 2018; Gao
142 et al., 2018; Yang et al., 2018) (Figs. 1 and 3). Previous work revealed that the continental margin of the
143 South China Sea is, structurally, highly segmented along strike (Franke, 2013; Savva et al., 2014; Zhao et
144 al., 2016; Yang et al., 2018). This along-strike segmentation is expressed by the variable bathymetry,
145 sediment thickness, structural styles and crustal structures the northern South China Sea reveals at present
146 (Figs. 1 and 3). Locally, the northern South China Sea comprises a number of crustal segments that are
147 divided on the basis of the age of the tectonic–metamorphic events that affected them (Ru and Pigott, 1986;
148 Franke, 2013; Savva et al., 2014). Two of those segments are relevant to this study; the northwest and the
149 northeast segments (Fig. 3).

150

151 *2.3.1 Northwest segment*

152

153 The northwest segment has a gentle topography and comprises a narrow continent–ocean transition
154 zone (Savva et al., 2014; Cameselle et al., 2015; Yang et al., 2018) (Figs. 1 and 3). It is characterised by a
155 series of tilted fault blocks blanketed by thick strata (Fig. 1e). Strata beneath Horizon T_g (top basement)
156 show chaotic, discontinuous internal reflections. The profile in Fig. 1e, spanning the continental shelf to the
157 deep-water realm, reveals a change from relatively large, widely spaced faults upslope to smaller normal
158 faults downslope, until a comparatively constant structure with no apparent faulting is imaged close to the
159 continent–ocean boundary (COB). Wide-angle OBS data published by Wu et al. (2012) suggests that the
160 crust thins markedly from north to south (Fig. 1c). As proposed by Savva et al. (2014) and Yang et al. (2018),
161 the northwest segment is characterised by a wide proximal domain and a narrow necking, or distal domain
162 (Fig. 3a). The crust beneath the northwest segment has also been significantly modified by Cenozoic
163 magmatism (Cameselle et al., 2015) (Fig. 1e).

164

165 *2.3.2 Northeast segment*

166

167 The BLFZ separates the northwest segment from a segment characterised by a wide region of rugged
168 topography (Figs. 1 and 3). This northeast segment comprises two widespread units separated by Horizon
169 T_g (top basement) from the shelf to the upper slope. These units include widespread, thick Mesozoic strata
170 (e.g. Well LF35-1-1) showing broad folds and thrust faults below Horizon T_g, and sub-parallel continuous
171 Cenozoic strata above (Fig. 1d). Compared to the northwest segment, continental crust on the lower
172 continental slope of the northeast segment was stretched to a greater degree, with listric normal faults

forming graben and half-graben basins (Fig. 1d). The northeast segment, therefore, is interpreted to coincide with the remnant Mesozoic forearc zone later deformed by Cenozoic continental rifting (Li et al., 2018; Yan et al., 2014).

The different amounts of extension accommodated by the northeast segment, when compared to its northwest counterpart, are revealed by its relatively wide necking (or distal) domain (Savva et al., 2014; Yang et al., 2018) (Fig. 3a). In addition, a high-velocity layer in the lower crust is suggested on wide-angle tomography and seismic reflection imagery (Nissen et al., 1995; Yan et al., 2001; Wang et al., 2006; Wei et al., 2011; Wan et al., 2017) (Fig. 1). This high-velocity layer is believed to be a localised feature, as it is not observed in the northwest segment (Fig. 1).

The above facts point to a significant change in crustal architecture between the northwest and the northeast segments of the South China Sea, with a transfer zone separating both (Savva et al., 2014; Cameselle et al., 2015; Yang et al., 2018) (Figs. 1 and 3). The marked structural boundary between the two segments occurs roughly at the Baiyun and Liwan Sags, which record unique extension modes, degrees of crustal thinning, degrees of magmatism and subsidence histories after the onset of continental breakup (Hu et al., 2009; Xie et al., 2014; Zhao et al., 2016).

3. Data and methods

This study uses multi-channel (2D) seismic data acquired by the China National Offshore Oil Corporation (CNOOC), and high-quality multibeam bathymetric data (Figs. 4-7). Multi-channel seismic lines were acquired by 576 channels with a shot-point spacing of 37.5 m and a common midpoint spacing of 12.5 m (Hu et al., 2009). Multibeam bathymetric data were processed using CaRIS HIPS (Li et al., 2014).

The multibeam dataset has a horizontal resolution of ~100 m and a vertical resolution of 3 m to 7 m in the study area (Zhao et al., 2014). It covers an area of approximately 70,000 km^2, spanning water depths of 100 m to 3500 m (Fig. 4).

The interpreted seismic profiles were gridded and imaged using IHS Kingdom® 8.7. Our interpretation workflow involved the systematic identification of fault patterns, key seismic horizons, and seismic-stratigraphic units bounded by these same horizons (Figs. 5 to 7). Faults were interpreted on multiple seismic lines with different orientations. We also produced isopach maps of key seismic units to trace syn-depositional fault activity and to recognise differing distribution patterns in Cenozoic strata (Figs. 4 and 8).

Submarine features in multibeam bathymetric data were interpreted based on their morphology. They were later tied to seismic data and published bathymetric information from the northern South China Sea (Figs. 4 and 8). Additional age controls and sedimentological data were provided by exploration wells BY2 and BY7-1, drilled in the study area, and by published sediment-core data from the northern South China Sea (Figs. 2 and 3).

4. Depositional architecture

Four regional unconformities, T_g (oldest) to T_4 (youngest), can be consistently traced across the study area (Figs. 5 to 7; Table 1). The oldest unconformity T_g (top basement, shown in red) coincides with the top of the Mesozoic basement (Figs. 5 to 7). High-amplitude, wavy seismic reflections in the lower continental crust were interpreted as the Main Liwan Detachment (MLD), which occurs beneath Horizon T_g in the Liwan Sag (Lei et al., 2018). Above Horizon T_g are deposited thick Cenozoic strata with continuous seismic reflections of variable amplitude. Unconformity T_7 (purple) is Early Oligocene in age and coincides with the

217 *breakup unconformity* in the Pearl River Mouth Basin and East Sub-basin (Briais et al., 1993; Zhao et al.,
218 2016; Sun et al., 2016) (Fig. 2). Horizon T_6 (blue) represents a Late Oligocene–Early Miocene unconformity
219 associated with the opening of the Southwest Sub-basin (Li et al., 2014; Sun et al; 2016; Zhao et al., 2016).
220 Horizon T_4 (green) represents the end of seafloor spreading in the East Sub-basin (Zhao et al., 2016).
221 Bounded by these four seismic horizons, three Cenozoic seismic units (Units 1 to 3) can be defined in the
222 study area (Fig. 2; Table 1).
223
224 *4.1* Unit 1 (Paleocene to Lower Oligocene)
225
226 Bounded at its base by Horizon T_g, and at its top by Horizon T_7, Unit 1 is observed as the basal seismic-
227 stratigraphic unit that overlies the acoustic basement (Figs. 5 to 7; Table 1). Unit 1 comprises syn-rift strata,
228 marking the principal period of tectonic subsidence and fault growth in the northern South China Sea (Figs.
229 5 to 7). On the structural high separating the Baiyun and Liwan Sags, Unit 1 shows chaotic seismic reflections
230 that are characteristic of magmatic bodies (Figs. 5 and 6).
231 Maximum basement depth is 8.31 s Two-Way Time (TWT) in the study area (Fig. 8a). The main
232 depocentre during the deposition of Unit 1, striking NE, is found in the central part of the Baiyun Sag (Fig.
233 8b). Within the Liwan Sag, rift geometry is characterised by a series of tilted crustal blocks bounded by
234 ocean-dipping normal faults, which detach and sole out in a large wavy basal detachment, the MLD (Lei et
235 al., 2018) (Fig. 5b). This basal detachment was disturbed by important magmatic activity in response to
236 rifting and continental breakup (Lei et al., 2018) (Fig. 5).

Stratigraphically, Unit 1 can be subdivided into three sub-units, 1A to 1C (Figs. 5c and 6b). Each sub-unit reflects distinct subsidence pulses and is separated by local stratigraphic unconformities (Figs. 5c and 6b).

4.2 Unit 2 (Late Oligocene to Early Miocene)

Unit 2 is bounded at its top by Horizon T_4 and at its base by Horizon T_7 (Figs. 5 to 7; Table 1). It represents Late Oligocene-Early Miocene deposition in the Pearl River Mouth Basin after continental rifting. It onlaps topographic highs and fills the depocentres between them (Figs. 5 to 7). In the Liwan Sag, isopach data for Unit 2 reveals major depocentres on the hanging-walls of Fault F1, F4 and F5 (Fig. 8a).

The recognition of a major erosional surface (T_6) across the study area allows Unit 2 to be divided into two sub-units (Units 2A and 2B). In Unit 2A, several chaotic and transparent packages are observed between continuous strata deposited on the hanging-wall block of Fault F4 (Fig. 5c). They are interpreted as recurrent mass-wasting deposits accumulated along faulted crustal blocks (e.g. Zhao et al., 2015). During the deposition of Unit 2A, the shelf break was located on the structural high between the Baiyun and Liwan Sags (Fig. 3b) (Han et al., 2016). However, this same shelf break migrated northwestwards into the northern part of Baiyun Sag during the deposition of Unit 2B (Han et al., 2016) (Fig. 3b).

4.3 Unit 3 (Middle Miocene to Holocene)

Bounded at its base by Horizon T_4, and at its top by the sea floor, Unit 3 represents drift strata and is Middle Miocene-Quaternary in age (Figs. 5 to 7; Table 1). The thickest sediments in Unit 3 occur in the

central part of the Baiyun Sag (Fig. 8b). Recurrent mass-transport deposits, imaged as highly discontinuous to chaotic strata over laterally continuous seismic reflections, are identified on the continental slope off the Dongsha Islands (see also Zhao et. al., 2015). On the eastern boundary of the Baiyun Sag, the presence of seafloor undulations offshore the Dongsha Islands is due to slow gravity-driven submarine creep (Li et al., 2016) (Figs. 4 and 6c). As a result, gravity flows controlled deposition on the northern continental slope by delivering sediment to discrete slope depocentres.

5. Structure, magmatism and timings of tectonic reactivation in the Baiyun-Liwan Fault Zone

5.1 Geometry of the Baiyun-Liwan Fault Zone (BLFZ)

The multibeam data in this work provides detailed morphological information from the BLFZ, imaging it as a complex area that is distinct from adjacent sedimentary basins and crustal blocks (Fig. 4). In addition, the deeply incised Pearl River Canyon occurs in the BLFZ, which is in itself located in a region of marked deformation between two volcanic arcs (Ding et al., 2013) (Figs. 4 and 6). The uneven surface above the BLFZ shows widespread slope instability and seafloor creep movements capable of transporting sediment into multiple slope depocentres (Figs. 4 and 6).

Interpretation of bathymetric and seismic data allowed us to define the region between F1, F2 and F5 as the structural and morphological expression of the BLFZ (Figs. 4 to 6). Here, the fault zone comprises a ~180 km wide negative flower structure located below the Baiyun and Liwan Sags, narrowing towards the southeast (Fig. 3b). It is ~220 km long and strikes NW-SE. In the BLFZ, numerous NE- and NW-striking

faults are identified at water depths between 100 m and 3500 m (Figs. 3, 5 and 9). These faults dip both to the east and west, and show important lateral reactivation (Figs. 3, 5 and 6).

The BLFZ shows five large faults that bound structural highs between main rift depocentres. These faults are broadly spaced and show large vertical offsets (Figs. 3, 5 and 7). Their strikes vary in the study area. The western border faults (blue) along the BLFZ are linear and strike to the NW (Figs. 3b, 5 and 7). To the east, faults (black) bounding the Mesozoic segment show NE and NW strikes (Figs. 3b and 8). Other minor faults are observed, but their continuity cannot be confirmed with accuracy. Numerous negative flower structures with very small offsets are identified within the BLFZ, suggesting the development of a broad zone of strike-slip movement (Figs. 5 and 6).

Seismic profiles crossing the BLFZ reveal that the larger faults are rooted in the lower crust, extending upwards from the basement into Unit 2 (Figs. 5 and 6). The interpreted seismic profiles also reveal significant Cenozoic deposition adjacent to, or within the BLFZ. In the Liwan Sag, maximum basement depth, and major depocenters in Units 1 and 2, are located close to F1, F4 and F5 (Fig. 8). Relatively thick *breakup sequences* sensu Soares et al. (2012), and a migration in the position of the shelf break towards the northwest, suggest deepening of the Liwan Sag after the Lower Oligocene (Fig. 8).

Bounded by the BLFZ, distinct crustal-scale structures are observed on each flank of the fault zone. The seismic profile in Fig. 7a crosses the lower slope of the northeast segment, and extends to the East Sub-basin. Here, the basement was intensely deformed by normal faults dipping both landwards and seawards, with the majority of faults offsetting strata up to Horizon T_6 (base Miocene) (Fig. 7a). Highly extended tilt blocks are observed (Fig. 7a).

Bounded to the west by the BLFZ, the northwest segment reveals a distinct mode of crustal deformation. Seismic profile Fig. 7b extends from the upper slope of the northwest segment to the Northwest Sub-basin.

Only a few normal faults with relatively small offsets are identified in this profile as propagating into Unit 3 (Middle Miocene-Quaternary) (Fig. 7b). The majority of these faults do not intersect the basement and often occur above igneous intrusions (Fig. 7b). Notably, the basement units in the northwest segment are intruded by multiple high-amplitude, igneous rocks (Fig. 7b).

5.2. Magmatism in the Baiyun-Liwan Fault Zone

Multibeam, 2D seismic reflection and borehole data reveal that the tectonic development of the BLFZ was accompanied by significant magmatism (Figs. 4, 6 and 8). A large-scale volcanic complex was identified at water depths of 500 m to 3000 m, covering an area of ~8000 km^2 (Fig. 3b). This volcanic complex comprises seamounts, igneous sills and intruded volcanic bodies (Figs. 5 and 6).

Two areas with abundant magmatic edifices are identified within the BLFZ (Figs. 3 and 4). The first area comprises a prominent seamount that rises 337 m above the sea floor, showing onlap terminations above horizon T_6 (Base Miocene) (Figs. 4 and 6b). This suggests an age of ~23.8 Ma for the seamount. The second area with magmatic edifices coincides with a topographic high on the modern sea floor (Fig. 4a).

In Unit 2 (Late Oligocene-Early Miocene), magmatic bodies comprise multiple discrete mounds, in places capped by carbonates, with underlying magmatic conduits fed by basalt magma (Zhao et al., 2016) (Figs. 5 and 6). Lateral and vertical facies variations reveal sedimentary features typical of hiatuses in local volcanism (Zhao et al., 2016). Igneous intrusions were also identified within Unit 3 (Middle Miocene-Quaternary), together with zones of chaotic or disrupted seismic reflections below intrusive bodies (Fig. 6c). It is worth noting that most magma deformed strata up to Horizon T_6 (Base Miocene) (Figs. 5 and 6).

5.3 Timing of fault reactivation

Variations in fault strikes and relative components of movement are observed in the BLFZ, with the bulk of faulting and deformation occurring during syn-rift extension (Figs. 3 and 8). The onset of continental rifting recorded the formation of long, large-offset boundary faults that generated fault-escarpments separating a rift trough from the northeast and northwest segments (Figs. 5 and 6). Local stratigraphic unconformities reveal multiple episodes of tectonic uplift and erosion along the footwalls of major faults (Figs. 4 to 6). These same unconformities indicate that the largest faults within the BLFZ were reactivated in multiple phases during continental rifting.

In Unit 2 (Late Oligocene-Early Miocene), NW-to NE-striking faults indicate that the BLFZ was active during the opening of the South China Sea (Figs. 3, 5 and 6). Significant mass-wasting in this unit was triggered by tectonic uplift and tilting of adjacent (faulted) blocks (Fig. 5c). The deformation style of these faults changed after continental breakup was initiated; extension shifted from large-offset boundary faults to widely-spaced boundary faults, accompanying an abrupt deepening of the sea floor. Hence, the geometry of faults and associated depocentres in Unit 2 reveal the generation of widespread accommodation space during multiple, diachronous episodes of seafloor spreading (Fig. 8c).

Above Horizon T_4 (base Middle Miocene), our data indicate that the eastern border faults were no longer active. In contrast, faulting in the western part of study area was long lived. Western border faults extend upwards to post-breakup strata (Figs. 5 and 6). Importantly, numerous extensional faults continue into the Late Neogene and Quaternary, together with transtensional structures, in the western part of the BLFZ (Figs. 6c and 6e).

6. Discussion

6.1 The Baiyun-Liwan Fault Zone: Role of tectonic inheritance in rifting and continental breakup

Previous studies indicate that the northwest and northeast segments of the South China Sea correlate with two distinct pre-Cenozoic basement terranes (Fig. 9). Along-strike differences between the northeast and northwest segments of the South China Sea are clear when comparing their structure and crustal architecture, suggesting a marked difference in pre-rift crustal composition (Figs. 1, 7 and 9). In addition, the location of extensional structures in the boundary between the two latter segments suggests that the BLFZ was formed over pre-existing structures that divided separate tectonic terrains prior to the rifting of the northern margin of the South China Sea. Such pre-existing structures were able to induce lateral variations in the rheology of the crust and mantle lithosphere, influencing the geometry of the continental margin and the style and distribution of deformation during Cenozoic rifting.

In the published literature, the northern South China Sea has been interpreted as evolving in relation to a homogeneous regional stress field generated during the Cenozoic by far-field extensional forces. A NW–SE extensional stress field is usually suggested for the northern South China Sea when combining evidence from the NE-trending syn-rift normal faults with the orientation of the seafloor spreading and the shapes of South China Sea conjugate margins (Taylor and Hayes, 1983; Briais et al., 1993; Franke, 2013; Li et al., 2014; Sun et al., 2016). However, our study reveals significant along-strike segmentation of the continental rifting process along the northern South China Sea (Figs. 1, 4 and 9). The main direction of extension within the BLFZ was not orthogonal to the rift axis during the Cenozoic. In fact, the BLFZ strikes obliquely to the predominant Cenozoic direction of extension, and the location of rift-related structures in this fault zone was

368 probably controlled by the reactivation of a (pre-Cenozoic) lithospheric weakness zone. The segmented
369 pattern of rift structures in the BLFZ thus resulted from the complex interplay between the regional stress
370 field imposed by continental rifting and local stresses generated along inherited weakness zones in the crust.
371 It is also likely that progressive extension of the continental lithosphere under prolonged oblique extensional
372 stresses was able to control faulting and subsequent volcano-tectonic events. Thus, the BLFZ represents a
373 broad deformation area accommodating spatial and temporal variations in rifting and continental breakup
374 across two different crustal segments.

375 Geophysical data reveals that continental crust was thinned in the study area to ~7 km (Hu et al., 2009),
376 a character demonstrating that the crust in the BLFZ experienced larger amounts of extension than adjacent
377 regions to the east and west. Based on these facts, another explanation for extreme crustal thinning of the
378 Baiyun and Liwan Sags can be proposed. We suggest that the Baiyun and Liwan Sags likely occur in a pre-
379 rift fault zone, having been strongly deformed and thinned prior to continental breakup. The Main Liwan
380 Detachment and isolated distributed extensional allochthons proposed by Lei et al. (2018), which indicate
381 prolonged thinning of pre-rift strata between Horizon T_g (top Basement) and the basal detachment, support
382 this interpretation (Fig. 5a).

383 Evidence from geophysical and borehole data suggests magmatic activity within the BLFZ was episodic
384 rather than continuous (Zhao et al., 2016). The first magmatic episode recorded in the BLFZ was
385 characterised by the extrusion and deposition of volcanic tuffs at ~35.5 Ma (Late Eocene) (Yan et al., 2006).
386 By combining data from exploration wells BY7-1 and BY2 with published seismic stratigraphic data, we
387 can identify a second volcanic episode, with multiple minor pulses, during the Early Miocene. This
388 volcanism was concomitant with the propagation of the ridge system to the southwest along the South China
389 Sea (Fig. 2). Despite the lack of exact chronostratigraphic dates to constrain a third episode of volcanism,

390 relatively younger igneous intrusions in the study area were emplaced after the end of seafloor spreading
391 (Fig. 6c).

392 This work suggests that Cenozoic volcanism and local uplift within the BLFZ are associated with
393 important lithospheric deformation in response to changes in the regional stress field, allowing at the same
394 time asthenospheric upwelling in response to lithospheric thinning. Given the evidence in this work that
395 Cenozoic magmatic bodies are confined within the BLFZ, we can postulate that magmatism in the northern
396 margin of the South China Sea was largely controlled by the (large-scale) faults mapped in this paper (Figs.
397 3 and 9).

398 The timing of fault zone reactivation can be constrained by analysing depositional systems and magma
399 bodies within the BLFZ (Figs. 4 and 8). Our study shows that the BLFZ was active during Cenozoic rifting
400 and subsequent post-rift compression. Deformation within the BLFZ was also complex, recording multiple
401 phases of extension. Reactivation events in the BLFZ are thus suggested to have generated vertical pathways
402 for the ascent of magma in the context of progressive continental breakup, thinned continental crust, and
403 tectonic-plate stress readjustments as the South China Sea was being formed (Fig. 9).

404

405 *6.2 Tectono-sedimentary evolution of the Baiyun-Liwan Fault Zone*

406

407 The BLFZ, extending through the Baiyun and Liwan Sags, comprises a wide area of deformation that
408 progressively controlled distinct rift systems (Fig. 8). Previous studies suggest that the Baiyun Sag is not a
409 classic half-graben basin; instead, it is characterized by NW- to E-striking syn-rift normal faults (Wang et
410 al., 2013; Zhou et al., 2018; Lei et al., 2018), associated with left-lateral transtension and continental rifting
411 (Wang et al., 2013). Nevertheless, a systematic investigation of strike-slip and shear sense indicators in the

area remains to be completed for the negative flower structures and earthquakes that occur within a broad area of oblique extension - more specifically along the western BLFZ (Wang et al., 2013) (Figs. 5 and 6).

A three-fold subdivision of the BLFZ's evolution is proposed here based on the interpretation of its architecture and structural evolution (Figs. 5-8; Table 1).

Stage I: Comprises the early deposition of syn-rift strata in the BLFZ, as documented by the wedge-shaped Unit 1 (Paleocene-Lowe Oligocene), and is correlated with the accumulation of syn-rift strata in the Pearl River Mouth Basin. Based on a detailed seismic stratigraphic interpretation of the syn-rift succession, three major episodes of crustal stretching are proposed in this work to reflect multi-phased continental rifting in the Pearl River Mouth Basin (Figs. 5 and 6; Table 1).

Stage II: Seismic and borehole data show important changes in the architecture of Unit 2 during Stage II (Figs. 5-6 and 8). From Early Oligocene to the Early Miocene, i.e. during the continental breakup of the South China Sea, the BLFZ was reactivated as a transfer zone, recording widespread (and diachronous) magma emplacement and tectonic uplift. The geometry of strata within Unit 2 (Late Oligocene-Early Miocene) also suggests widespread deepening of the BLFZ during continental breakup. The accommodation space created in the vicinity of the BLFZ was followed by rapid (and significant) sedimentation. Based on geophysical evidence, the shelf break migrated to the northern part of Baiyun Sag at 23.8 Ma, with subsequent initiation of the Pearl River Canyon erosion on the continental slope (Ding et al., 2013). This age corresponds to the propagation of ocean spreading from the East to the Southwest Sub-basin (Li et al., 2014; Sun et al., 2016). In the study area, the boundary between Units 1 and 2 is marked by a shift from the localized infill of discrete syn-rift basins to more widespread deposition in the Pearl River Mouth Basin (Figs. 5 and 8).

Stage 3: Following sediment progradation during the deposition of breakup sequences in Unit 2, lower energy conditions prevailed during the deposition of Unit 3 (Middle Miocene-Quaternary) in the drift stage (Figs. 5-8). The BLFZ recorded faulting and magmatism after the Middle Miocene, providing evidence for its importance within an overall transtensional setting. In Unit 3, the northern and northeastern continental slopes of the BLFZ were modified by features such as submarine canyons, submarine slides, and seafloor creep zones, suggesting that the drift succession comprises strata deposited by complex downslope and along-slope processes (Ding et al., 2013; Li et al., 2014; Li et al., 2016) (Figs. 4 and 6). The BLFZ also controlled the incision of the Pearl River Mouth Canyon from the shelf break to the distal margin. We therefore suggest that the Pearl River Mouth Canyon, and the BLFZ, formed efficient conduits for sediment bypassing the continental slope towards the ocean basins during the deposing of Unit 3, i.e. during the Middle Miocene-Quaternary (Figs. 4 and 9).

Widespread magmatism, and the landward migration of the shelf break in the BLFZ, indicate that fault displacement peaked at ~23.8 Ma, a date corresponding to the propagation of seafloor spreading from the East to the Southwest Sub-basin (Zhao et al., 2016) (Fig. 8). As a result, the BLFZ is shown in this work to be the preferred strike-slip domain where continental crust accommodated crustal movements during rifting and continental breakup in the northern South China Sea (Fig. 9). Furthermore, the presence of long strike-slip faults, modern earthquake activity and the Baiyun Slide Complex, all suggest that the modern BLFZ is a region of important geohazards, particularly close to alternating releasing–restraining fault bends that formed along its length (Li et al., 2014).

7. Conclusions

From the detailed analysis of multibeam, multi-channel seismic and borehole data, we reach the following conclusions:

1. A newly discovered Baiyun-Liwan Fault Zone (BLFZ), located in the northern South China Sea, is analysed for the first time in this work. The BLFZ, broadly striking NW to NE, comprises a ~220 km-long, ~180 km-wide strike-slip zone of deformation, oblique to the continental margin. The BLFZ is a first-order transfer zone that accommodated significant intra-plate deformation during the diachronous rifting and opening of the South China Sea, and was accompanied by episodic magmatism.
2. The BLFZ is likely derived from an inherited Mesozoic lithospheric-scale weakness zone in the crust, and was subsequently reactivated following the onset of Cenozoic extension in the South China Sea. Distinct crustal-scale structures observed on each flank of the fault zone highlight the importance of pre-existing weak zones in the evolution of continental rift systems. Significant crustal thinning was also recognised within the fault zone, a character we consider to have favoured prolonged magma emplacement. Our results thus show that the BLFZ played an important role in segmenting the northern continental margin of the South China Sea along its strike.
3. Our study reveals that pre-rift tectonics created pre-existing heterogeneities with variable orientation in the basement, which controlled the initial rift evolution. The progressive thinning of the continental lithosphere under constant, prolonged oblique extension controlled rift propagation roughly in a NW–SE direction. Vertical crustal movements in the BLFZ reached their peak during the Early Miocene. At the same time, the fault zone accommodated motion and strain resulting from the propagation of seafloor spreading from northeast to southwest in the South China Sea.
4. The interpreted multibeam bathymetry and seismic data show that NW–SE to NE–SW faults within the

BLFZ control the morphology of the study area at present. Thus, the Late Miocene–Quaternary incision of the Pearl River Canyon has a structural relationship with the BLFZ forming, at present, a major area of sediment bypass towards ocean basins in the South China Sea. The incision of the Pearl River Canyon indicates that the drift successions in the BLFZ depend in great part on the evolution of this latter sediment fairway.

5. The occurrence of intense faulting and earthquake clusters in the BLFZ suggests it comprises an area of significant geohazards at present. Hence, this is an important case-study showing that palaeogeographic reconstructions on divergent margins must take into account not only the older rift-related strain accommodation, but also the variable transcurrent deformation that transfer zones record well after continental breakup was achieved.

Acknowledgements

This study was supported by the National Natural Science Foundation of China (Nos. 41706054, U1701641 and 41876054), National Natural Science Foundation of Guangdong Province (2017A030310340) and Science Foundation of Key Laboratory of Ocean and Marginal Sea Geology, CAS (OMG18-06). The authors are grateful to China National Offshore Oil Company for providing the data and permission to publish this paper. We would like to thank G. Manatschal, G. Mohn and M. Nirrengarten for their constructive comments, which greatly improved this paper. The authors thank the editor J.P. Avouac and the reviewer A. Briais and two anonymous reviewers for their valuable contribution in improving this paper.

References

Briais, A., Patriat, P., Tapponnier, P., 1993. Updated interpretation of magnetic anomalies and seafloor spreading stages in the South China Sea: implications for the Tertiary tectonics of Southeast Asia. J. Geophys. Res. 98, 6299–6328.

499 Buck, W.R., 1991. Modes of continental lithospheric extension. J. Geophys. Res. Solid Earth 96, 20161–20178.

500 Cameselle, A. L., Ranero, C. R., Franke, D., Barckhausen, U., 2015. The continent-ocean transition on the northwestern South China Sea, Basin Res., 28(3), 1–
501 23, doi:10.1111/bre.12137.

502 Chen, H.Z., Wu, X.J., Zhou, D., Wang, W.Y., Hao, H.J., 2005. Meso-Cenozoic faults in Zhujiang River Mouth Basin and their geodynamic background, Journal
503 of Tropical Oceanography, 24(2), 52-61. doi:10.3969/j. issn.1009-5470.2005.02.007

504 Corti, G., 2008. Control of rift obliquity on the evolution and segmentation of the main Ethiopian rift. Nat. Geosci. 1, 258–262.

505 Ding, W., Li, J., Li, J., Fang, Y., Tang, Y., 2013. Morphotectonics and evolutionary controls on the Pearl River Canyon system, South China Sea. Mar. Geophys.
506 Res. 34, 221–238. http://dx.doi.org/10.1007/s11001-013-9173-9.

507 Dunbar, J.A., Sawyer, D.S., 1989. How preexisting weaknesses control the style of continental breakup. J. Geophys. Res. 94 (B6), 7278–7292.

508 Festa, A., Balestro, G., Borghi, A., De Caroli, S., Succo, A., 2019. The role of structural inheritance in continental break-up and exhumation of Alpine Tethyan
509 mantle (Canavese Zone, Western Alps). Geoscience Frontiers https://doi.org/10.1016/j.gsf.2018.11.007 (online version).

510 Fan, C., Xia, S., Cao, J., Zhao, F., Sun, J., Wan, K., Xu, H., 2019. Lateral crustal variation and post-rift magmatism in the northeastern South China Sea determined
511 by wide-angle seismic data. Mar. Geol. 410, 70–87.

512 Franke, D., 2013. Rifting, lithosphere breakup and volcanism: comparison of magma poor and volcanic rifted margins. Mar. Pet. Geol. 43, 63–87.

513 Gao, J., Peng, X., Wu, S., Lüdmann, T., McIntosh, K., Ma, B., Xu, Z., 2018. Different expressions of the crustal structure across the Dongsha Rise along the
514 northeastern margin of the South China Sea. J. Asian Earth Sci. in press.

515 Han, J., Xu, G., Li, Y., Zhuo, H., 2016. Evolutionary history and controlling factors of the shelf breaks in the Pearl River Mouth Basin, northern South China
516 Sea. Mar. Pet. Geol. 77, 179-189.

517 Hu, D., Zhou, D., Wu, X., He, M., Pang, X., Wang, Y., 2009. Crustal structure and extension from slope to deepsea basin in the northern South China Sea. J. Earth
518 Sci. 20, 27–37.

519 Jackson, J.A., Gagnepain, J., Housman, G., King, G., Papadimitriou, P., Soufleris, P., and Virieux, J., 1982, Seismicity, normal faulting and the geomorphological
520 development of the Gulf of Corinth (Greece): The Corinth earthquakes of February and March 1981: Earth Planet. Sci. Lett. 57, 377–397, doi:10.1016/0012-
521 821X(82)90158-3.
522 Lei, C., Alves, T.M., Ren, J., Pang, X., Yang, L., Liu, J., 2019. Depositional architecture and structural evolution of a region immediately inboard of the locus of
523 continental breakup (Liwan Sub-basin, South China Sea). Geol. Soc. Am. Bull. https://doi.org/10.1130/B35001.1.
524 Li, C.F., Xu, X., Lin, J., Sun, Z., et al., 2014. Ages and magnetic structures of the South China Sea constrained by the deep tow magnetic surveys and IODP
525 Expedition 349. Geochem. Geophys. Geosyst. 15, 4958–4983.
526 Li, W., Wu, S., Völker, D., Zhao, F., Mi, L., Kopf, A., 2014. Morphology, seismic characterization and sediment dynamics of the Baiyun Slide Complex on the
527 northern South China Sea margin. J. Geol. Soc. (Lond.) 171, 865–877.
528 Li, W., Alves, T. M., Wu, S.G., Rebesco, M., Zhao, F., Mi, L.J., Ma, B.J., 2016. A giant, submarine creep zone as a precursor of large-scale slope instability
529 offshore the Dongsha Islands (South China Sea). Earth Planet. Sci. Lett. 451, 272–284.
530 Li, F., Sun, Z., Yang, H., 2018. Possible spatial distribution of the Mesozoic volcanic arc in the present-day South China Sea continental margin and its tectonic
531 implications. J. Geophys. Res. Solid Earth, 123. https://doi.org/10.1029/2017JB014861
532 Manatschal, G., 2004. New models for evolution of magma-poor rifted margins based on a review of data and concepts from West Iberia and the Alps. Int. Jour.
533 Earth Sci. 93, 432-466.
534 Manatschal, G., Lavier, L., Chenin, P., 2015. The role of inheritance in structuring hyperextended rift systems: some considerations based on observations and
535 numerical modeling. Gondwana Res. 27 (1), 140-164. http://dx.doi.org/10.1016/ j.gr.2014.08.006.
536 McIntosh, K., van Avendonk, H., Lavier, L., Lester, W. R., Eakin, D., Wu, F., Liu, C.-S., Lee, C.-S., 2013. Inversion of a hyper-extended rifted margin in the
537 southern Central Range of Taiwan, Geology 41(8), 871–874, doi:10.1130/G34402.1.
538 Morley, C. K., 2010. Stress re-orientation along zones of weak fabrics in rifts: An explanation for pure extension in ‘oblique’ rift segments? Earth Planet. Sci.
539 Lett. 297, 667–673. doi:10.1016/j.epsl.2010.07.022.

Nissen, S.S., Hayes, D.E., Buhl, P., Diebold, J., Yao, B., Zeng, W., Chen, Y., 1995. Deep penetrating seismic sounding across the northern margin of the South China Sea. J. Geophys. Res. Solid Earth 100 (B11), 22407–22433.

Pereira, R., Alves, T.M., 2013. Crustal deformation and submarine canyon incision in a Meso-Cenozoic first-order transfer zone (SW Iberia, North Atlantic Ocean). Tectonophysics, 601, 148-162.

Peron-Pinvidic, G., Manatschal, G., Minshull, T.A., Sawyer, D.S., 2007. Tectonosedimentary evolution of the deep Iberia-Newfoundland margins: evidence for a complex breakup history. Tectonics 26, doi:10.1029/2006tc001970.

Petersen, K.D., Schiffer, C., 2016. Wilson cycle passive margins: control of orogenic inheritance on continental breakup. Gondwana Research 39, 131–144.

Philippon, M., Willinghofer, E., Sokoutis, D., Corti, G., Sani, F., Bonini, M., Cloetingh, S., 2015. Slip re-orientation in oblique rifts. Geology 43, 147-150.

Piqué, A., Laville, E., 1996. The Central Atlantic rifting: reactivation of Palaeozoic structures? J. Geodyn. 21, 235–255.

Ring, U., 1994. The influence of preexisting structure on the evolution of the Cenozoic Malawi rift (East African rift system). Tectonics 13, 313–326.

Ru, K., Pigott, J.D., 1986. Episodic rifting and subsidence in the South China Sea, AAPG Bull., 70, 1136–1155.

Savva, D., Pubellier, M., Franke, D., Chamot-Rooke, N., Meresse, F., Steuer, S., Auxietre, J.L., 2014. Different expressions of rifting on the South China Sea margins. Mar. Pet. Geol. 58, 579–598.

Shao, L., Cao, L., Qiao, P., Zhang, X., Li, Q., van Hinsbergen, D.J., 2017. Cretaceous–Eocene provenance connections between the Palawan Continental Terrane and the northern South China Sea margin. Earth Planet. Sci. Lett. 477, 97-107.

Sun, X.M., Zhang, X.Q., Zhang, G.C., Lu, B.L., Yue, J.P., Zhang, F., 2014. Texture and tectonic attribute of Cenozoic basin basement in the northern South China Sea. Science China: Earth Sciences, 57: 1199–1211, doi: 10.1007/s11430-014-4835-2.

Sun, Z., Stock, J., Jian, Z., McIntosh, K., Alvarez-Zarikian, C.A., Klaus, A., 2016. Expedition 367/368 Scientific Prospectus: South China Sea Rifted Margin. International Ocean Discovery Program. http://dx.doi.org/10.14379/iodp.sp.367368.2016.

Taylor, B., Hayes, D.E., 1983. Origin and history of the South China Sea basin. Washington DC American Geophysical Union Geophysical Monograph 27, 23-56.

561 Tommasi, A., Vauchez, A., 2001. Continental rifting parallel to ancient collisional belts: an effect of the mechanical anisotropy of the lithospheric mantle. Earth
562 Planet. Sci. Lett. 185, 199 – 210.
563 Van Wijk, J., 2005. Role of weak zone orientation in continental lithosphere extension. Geophys. Res. Lett. 32, L02303.
564 Wan, K., Xia, X., Cao, J., Sun, J., Xu, H., 2017. Deep seismic structure of the northeastern South China Sea: Origin of a high-velocity layer in the lower crust, J.
565 Geophys. Res. Solid Earth, 122, doi:10.1002/2016JB013481.
566 Wang, T., Chen, M., Lee, C., Xia, K., 2006. Seismic imaging of the transitional crust across the northeastern margin of the South China Sea. Tectonophysics 412,
567 237–254.
568 Wei, X.D., Ruan, A.G., Zhao, M.H., Qiu, X.L., Li, J.B., Zhu, J.J., Wu, Z.L., Ding, W.W., 2011. A wide-angle OBS profile across Dongsha Uplift and Chaoshan
569 Depression in the midnorthern South China Sea. Chin. J. Geophys. (Chin. Ed.) 54 (6), 1149–1160.
570 Wu, Z.L., Li, J.B., Ruan, A.G., Lou, H., Ding, W.W., Niu, X.W., Li, X.B., 2012. Crustal structure of the northwestern sub-basin, South China Sea: results from a
571 wide-angle seismic experiment. Science China Earth Sciences 55, 159–172. http://dx.doi.org/10.1007/s11430-011-4324-9.
572 Wu, S., Gao, J., Zhao, S., Lüdmann, T., Chen, D., Spence, G., 2014. Post-rift uplift and focused fluid flow in the passive margin of northern South China Sea.
573 Tectonophysics 615, 27-39.
574 Xie, H., Zhou, D., Li, Y.P., Pang, X., Li, P.X., Chen, G.H., Li, F.C., Cao, J.H., 2014. Cenozoic tectonic subsidence in deepwater sags in the Pearl River Mouth
575 Basin, northern South China Sea. Tectonophysics 615–616, 182–198.
576 Yan, P., Zhou, D., Liu, Z., 2001. A crustal structure profile across the northern continental margin of the South China Sea. Tectonophysics 338, 1–21.
577 Yan, P., Deng, H., Liu, H., Zhang, Z., Jiang, Y., 2006. The temporal and spatial distribution of volcanism in the South China Sea region. J. Asian Earth Sci. 27,
578 647–659.
579 Yan, P., Wang, L., Wang, Y., 2014. Late Mesozoic compressional folds in Dongsha Waters, the northern margin of the South China Sea, Tectonophysics 615,
580 213–223, doi:10.1016/j.tecto.2014.01.009.
581 Yang, L., Ren, J., McIntosh, K., Pang, X., Chao, L., Zhao, Y., 2018. The structure and evolution of deepwater basins in the distal margin of the northern South
582 China Sea and their implications for the formation of the continental margin. Mar. Pet. Geol. 92, 234-254.

583 Zhao, F., Wu, S.G., Sun, Q.L., Huuse, M., Li, W., Wang, Z.J., 2014. Submarine volcanic mounds in the Pearl River Mouth Basin, northern South China Sea. Mar.
584 Geol. 355, 162–172.
585 Zhao, F., Alves, T.M., Li, W., Wu, S., 2015. Recurrent slope failure enhancing source rock burial depth and seal unit competence in the Pearl River Mouth Basin,
586 offshore South China Sea. Tectonophysics 643, 1–7.
587 Zhao, F., Alves, T.M., Wu, S.G., Li, W., Huuse, M., Mi, L.J., Sun, Q.L., Ma, B.J., 2016. Prolonged post-rift magmatism on highly extended crust of divergent
588 continental margins (Baiyun Sag, South China Sea). Earth Planet. Sci. Lett. 445, 79–91.
589 Zhou, D., Sun, Z., Chen, H. Z., Xu, H. H., Wang, W. Y., Pang, X., Cai, D. S., Hu, D. K., 2008. Mesozoic paleogeography and tectonic evolution of South China
590 Sea and adjacent areas in the context of Tethyan and paleo-Pacific interconnections, Island Arc, 17(2), 186–207, doi:10.1111/j.1440-1738.2008.00611.x.

591 **Figures**

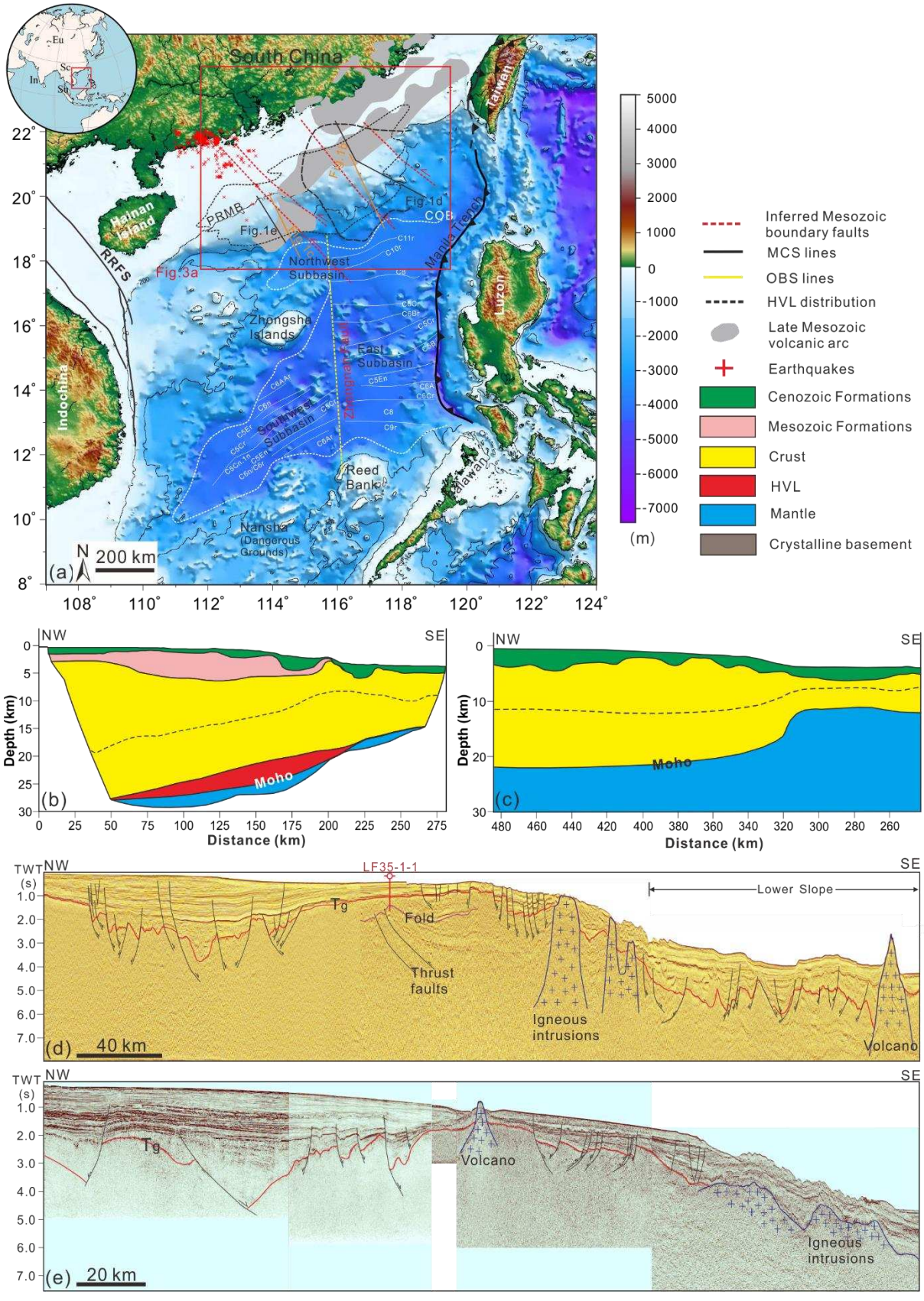

592

Fig. 1. (a) Combined topographic and bathymetric maps of the northern South China Sea (see location map in inset) showing the distribution of major faults based on gravity data (Chen et al., 2005), the location of the Mesozoic volcanic arc in the northern South China Sea, and the distribution of a high velocity layer (HVL) identified in previous work (Nissen et al., 1995; Yan et al., 2001; Wang et al., 2006; Wei et al., 2011; Yan et al., 2014; Wan et al., 2017). The box marks the location of Figs. 3a. The locations of the Pearl River Mouth Basin (PRMB) and main geomorphological features are labelled. (b) and (c) Velocity profiles crossing the northern South China Sea (see location in Fig.1a) showing differences in the crustal structure between its northeast and northwest segments (Fan et al., 2019; Wu et al., 2012). The Cenozoic layer is characterised by velocities of ~2.0–3.5 km/s, the Mesozoic layer by velocities over ~3.5 km/s–5.5 km/s, and the crustal layer by velocities over ~5.5 km/s–7.5 km/s. Upper mantle velocities are >7.5 km/s. (d) and (e) Regional seismic profiles crossing the northern South China Sea (see location in Fig.1a) showing the geometry of sedimentary basins in the northeast and northwest segments defined in this work (after Gao et al., 2018). COB - continent–ocean boundary; RRFS - Red River Fault System. HVL - high-velocity layer; OBS - ocean bottom seismograph; MCS - multi-channel seismic profiles.

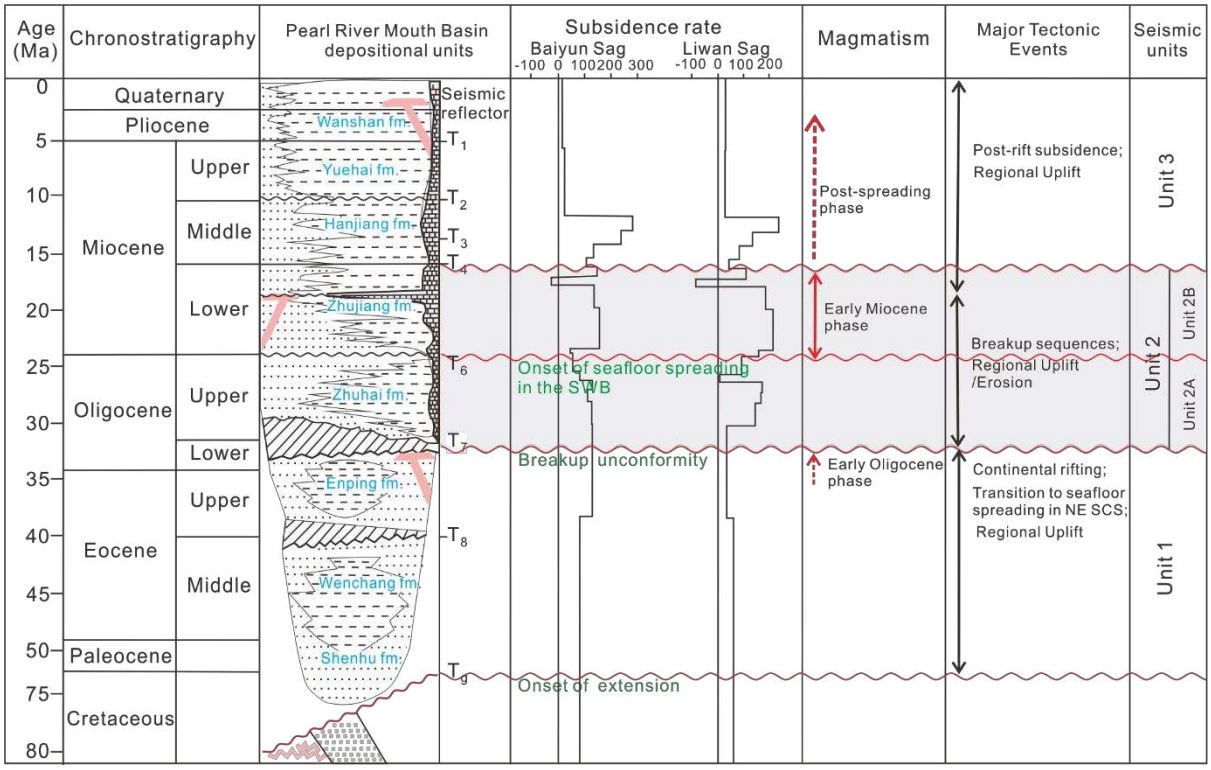

Fig. 2. Stratigraphic column of the Pearl River Mouth Basin showing regional lithostratigraphic units together with the main tectonic and magmatic events affecting the study area since the Cretaceous. The column is modified after Zhao et al. (2016).

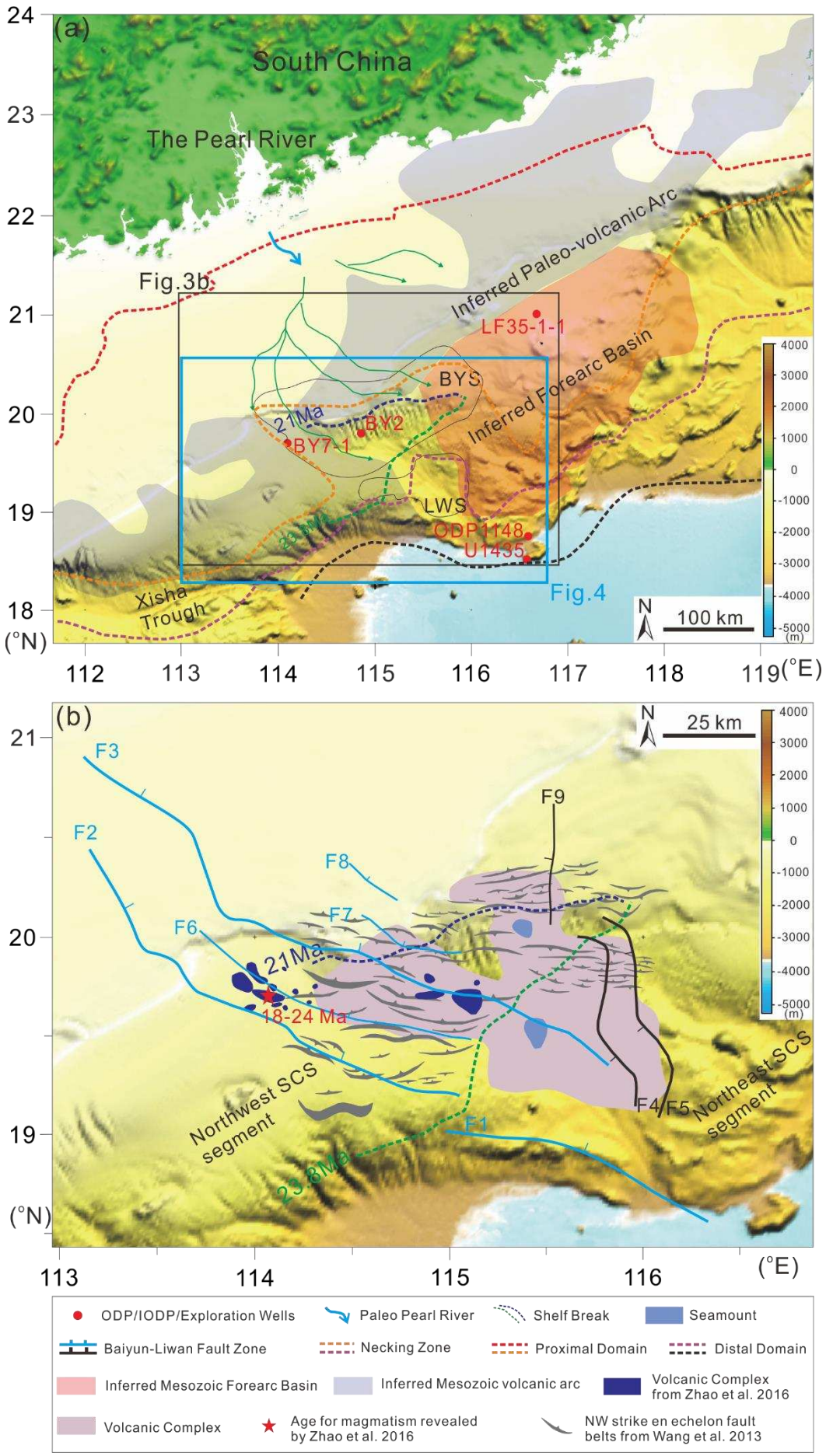
(a)
South China
The Pearl River
Fig.3b
Inferred Paleo-volcanic Arc
LF35-1-1
BYS
Inferred Forearc Basin
21Ma
BY2
BY7-1
LWS
ODP1148
U1435
23 Ma
Fig.4
Xisha Trough
N
100 km
4000
3000
2000
1000
0
-1000
-2000
-3000
-4000
-5000
(m)
24
23
22
21
20
19
18
(°N)
112
113
114
115
116
117
118
119(°E)
(b)
N
25 km
F3
F2
F9
F8
F7
F6
21Ma
18-24 Ma
Northwest SCS segment
F4/F5
Northeast SCS segment
F1
23.8Ma
21
20
19
(°N)
113
114
115
116
(°E)
ODP/IODP/Exploration Wells
Paleo Pearl River
Shelf Break
Seamount
Baiyun-Liwan Fault Zone
Necking Zone
Proximal Domain
Distal Domain
Inferred Mesozoic Forearc Basin
Inferred Mesozoic volcanic arc
Volcanic Complex from Zhao et al. 2016
Volcanic Complex
Age for magmatism revealed by Zhao et al. 2016
NW strike en echelon fault belts from Wang et al. 2013

620

Fig. 3. (a) Structural setting of the Pearl River Mouth Basin (see location in Fig.1) showing Mesozoic units and the positions of the shelf break in different evolutionary stages (see Han et al., 2016; Li et al., 2018). The locations of exploration wells and IODP/ODP sites are labelled. Note the shelf break migrated landwards from 23.8 Ma (green dashed line) to 21 Ma (dark blue dashed line). (b) Structural map showing the distribution of major faults and magmatic features in the Baiyun-Liwan Fault Zone (BLFZ) over the interpreted basement horizon T_g. The blue and black solid lines show the western and eastern border faults, respectively. NW-striking en echelon faults (grey solid lines) recognised in Wang et al. (2013) are also shown. Note the widespread magmatism recorded in the BLFZ. SCS - South China Sea; BYS - Baiyun Sag; LWS - Liwan Sag; IODP - International Ocean Discovery Program; ODP - Ocean Drilling Project.

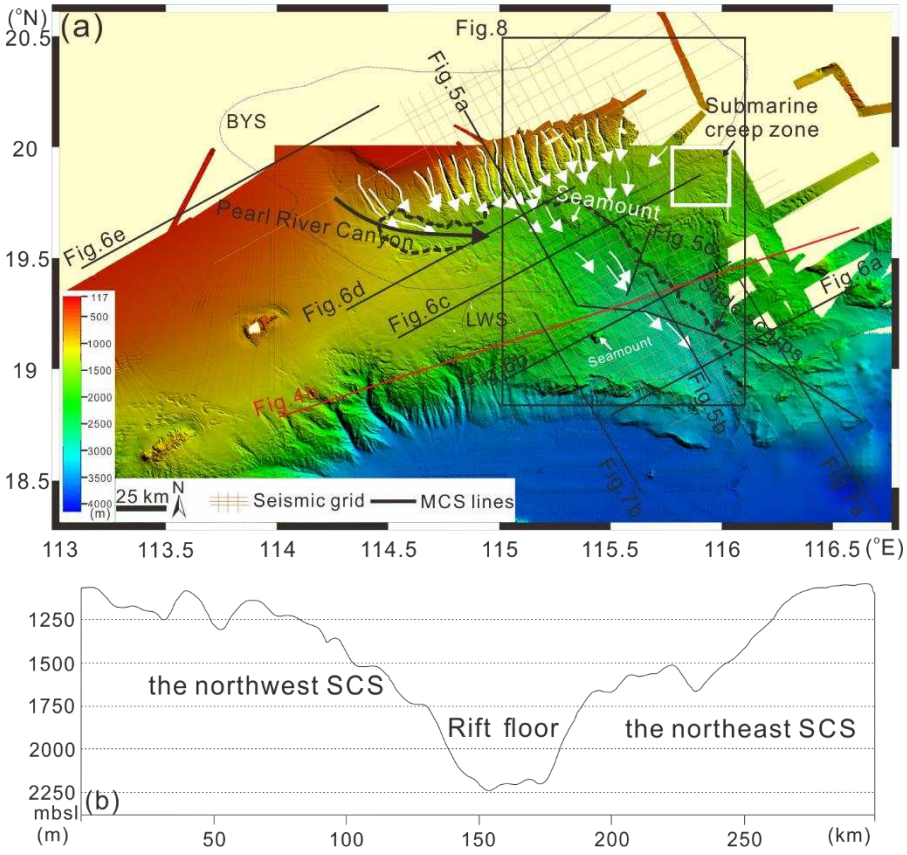

Fig. 4. (a) Multibeam bathymetric map (see location in Fig. 3a) revealing the detailed morphology of the study area. The orange solid lines indicate the locations of multichannel seismic reflection profiles used. The black solid

634 lines mark the locations of multi-channel seismic profiles discussed in this work. The red solid line highlights the

635 location of Figs. 4b. Note the incision of the Pearl River Canyon and the widespread gravity flows observed in

636 the study area. (b) Bathymetric profile across the BLFZ (see location in Fig.4a).

637

638

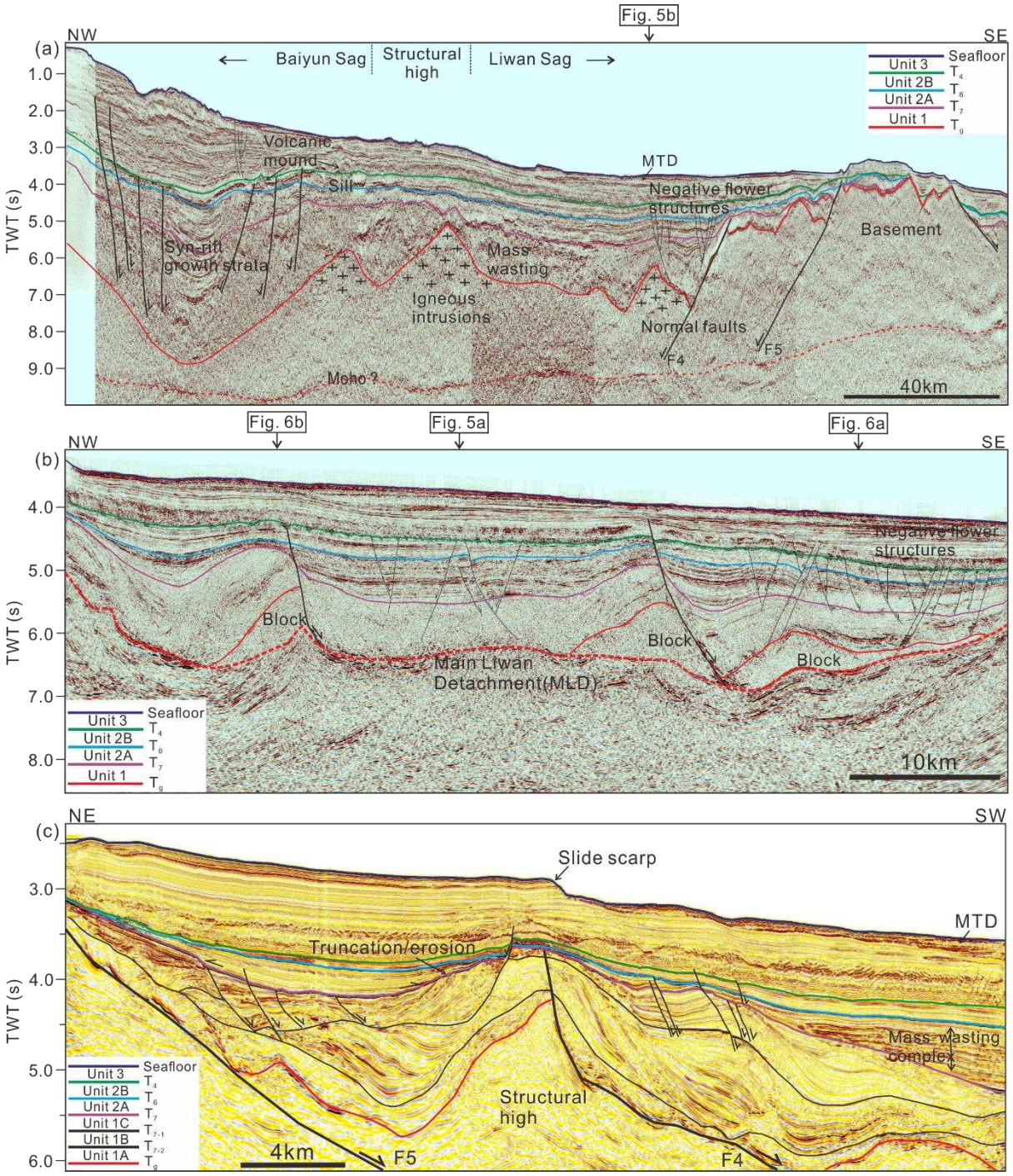

639

Fig. 5. (a) Seismic profile across the northern South China Sea showing interpreted structural and stratigraphic relationships in the BLFZ. See location of the seismic profile in Fig. 4a. The eastern flank of Liwan Sag is bounded by NW- to NE-striking faults. Three tectono-stratigraphic units were interpreted in the PRMB; Units 1 to 3. (b) Interpreted north-south seismic profile from the Liwan Sag showing numerous negative flower structures within Units 1 and 2. See location of the seismic profile in Fig. 4a. (c) Interpreted seismic profile highlighting the prominent SW-dipping Unit 1 and local thinning and erosion in Units 1 and 2 over the fault zone. See location of the seismic profile in Fig. 4a. Note the marked erosion and truncation of sediments below Horizon T_7 (Lower Oligocene) and the mass-wasting complex observed in Unit 2 to the southwest.

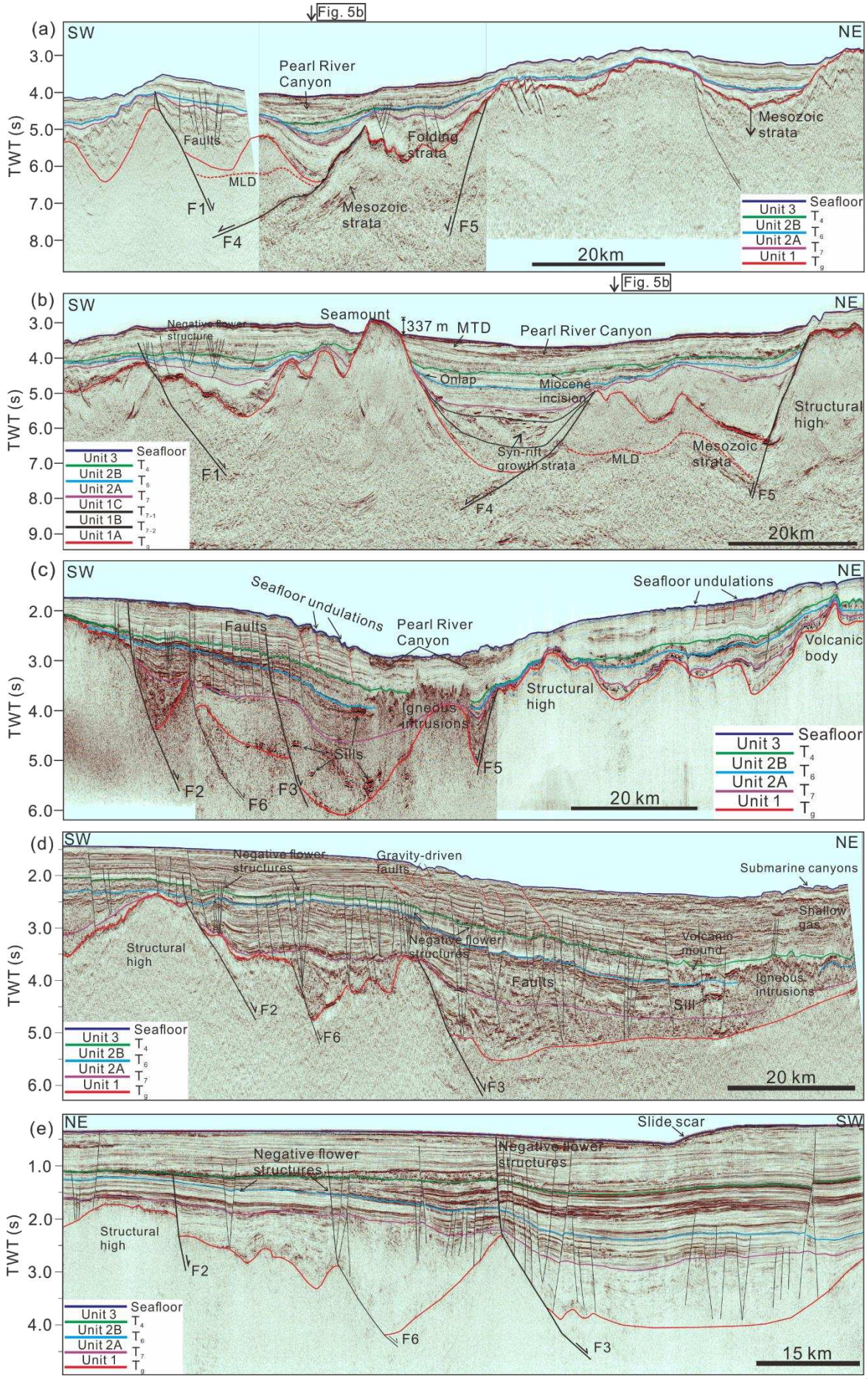
(a)
SW
NE
Fig. 5b
Pearl River Canyon
Faults
MLD
F1
F4
Mesozoic strata
Folding strata
F5
Mesozoic strata
20km
Unit 3
Unit 2B
Unit 2A
Unit 1
Seafloor
TWT (s)
(b)
SW
NE
Fig. 5b
Negative flower structure
Seamount
337 m
MTD
Pearl River Canyon
Onlap
Miocene incision
Structural high
Syn-rift growth strata
MLD
Mesozoic strata
F1
F4
F5
20km
Unit 3
Unit 2B
Unit 2A
Unit 1C
Unit 1B
Unit 1A
Seafloor
(c)
SW
NE
Seafloor undulations
Faults
Pearl River Canyon
Seafloor undulations
Volcanic body
Structural high
Igneous intrusions
Sills
F2
F6
F3
F5
20 km
Unit 3
Unit 2B
Unit 2A
Unit 1
Seafloor
(d)
SW
NE
Negative flower structures
Gravity-driven faults
Submarine canyons
Shallow gas
Structural high
Negative flower structures
Volcanic mound
Faults
Igneous intrusions
Sill
F2
F6
F3
20 km
Unit 3
Unit 2B
Unit 2A
Unit 1
Seafloor
(e)
NE
SW
Slide scar
Negative flower structures
Negative flower structures
Structural high
F2
F6
F3
15 km
Unit 3
Unit 2B
Unit 2A
Unit 1
Seafloor

648

649 Fig. 6. (a) and (b) Multi-channel seismic profiles across the Liwan Sag showing the geometry of the BLFZ. See
650 location of the seismic profile in Fig. 4a. Note the differences in sedimentary architecture in both sides of the
651 BLFZ and the onlap geometries observed on the flanks of the seamount. (c) Interpreted seismic profile across the
652 central portion of the study area (see Fig. 4a for location) showing intense igneous intrusions within Unit 3. (d)
653 and (e) Interpreted multichannel 2D seismic profiles across the eastern Baiyun Sag showing widespread negative
654 flower structures in the BLFZ. Note the occurrence of igneous bodies, seafloor undulations, intense faulting and
655 deposition of mass-transport deposits on both flanks of the fault zone. See location of the seismic profile in Fig.
656 4a.
657

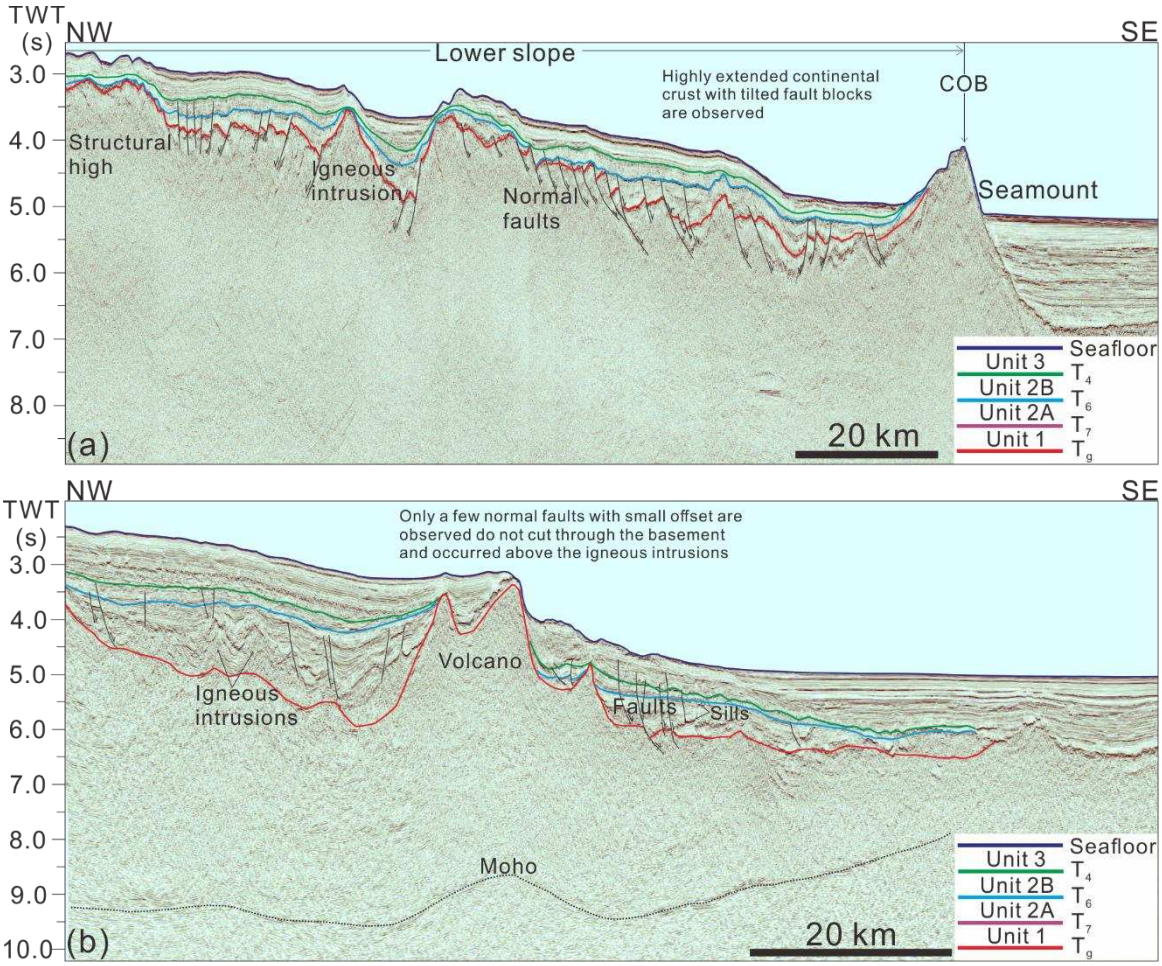

658

659 Fig. 7. (a) Interpreted seismic profile across the lower slope of the northeast. See location of the seismic profile

in Fig. 4a. (b) Interpreted multichannel 2D seismic profile across the slope of the northwest segment of South China Sea (see Fig. 4a for location). Note the difference of crustal structure and extension mode between the two segments imaged above. COB - continent–ocean boundary

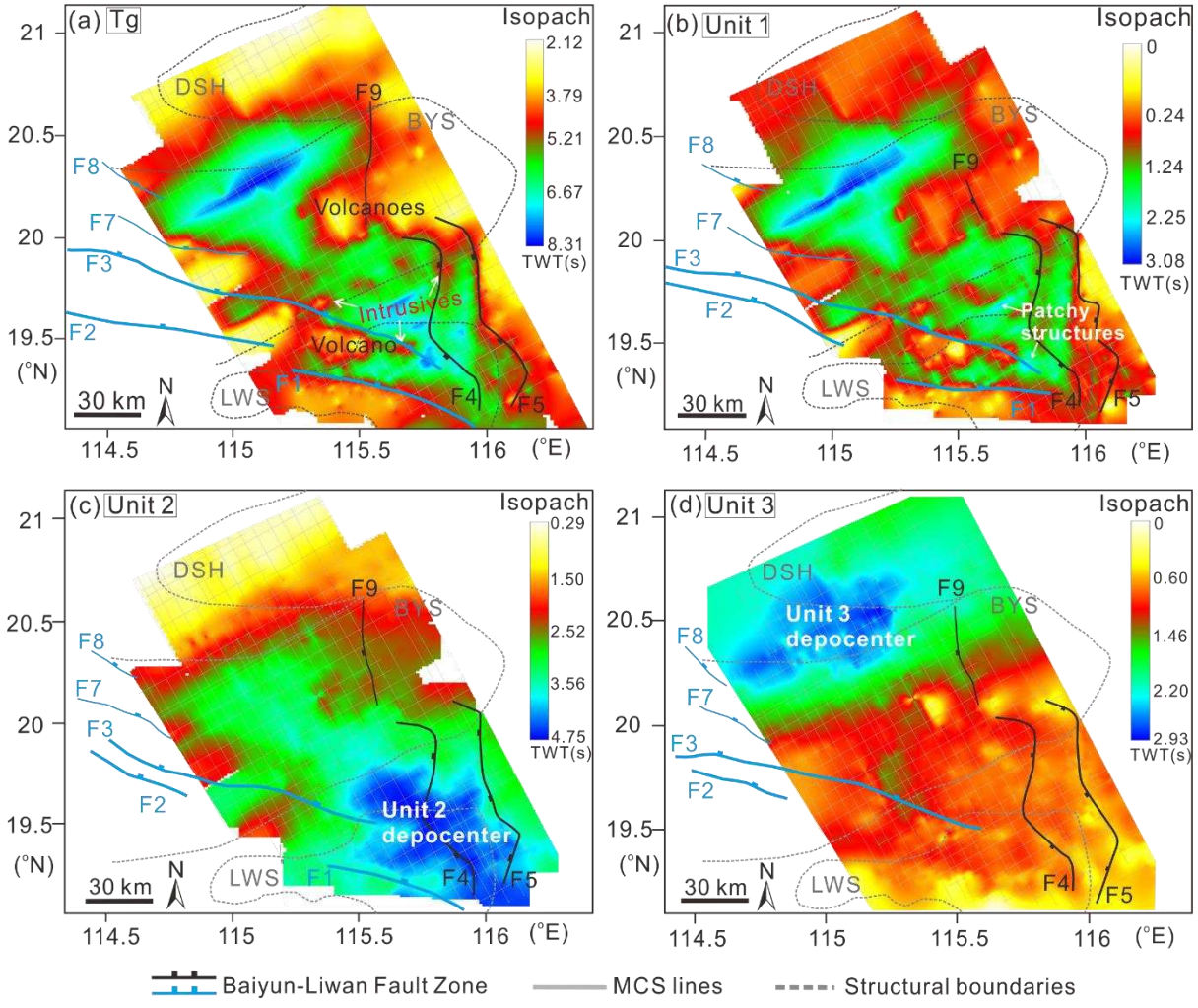

Fig. 8. (a) TWT structural map showing the depth of basement within the BLFZ. Widespread volcanic bodies interspersed throughout the fault zone are revealed. (b), (c) and (d) Isopach thickness maps showing the variations in sediment thickness (seconds TWT) in stratigraphic Units 1 to 3. The maps also show the fault patterns interpreted on T_g, T_7, T_6 and T_4. Note that the Cenozoic depocentres have migrated landwards since the Early Miocene. DSH - Dongsha High.

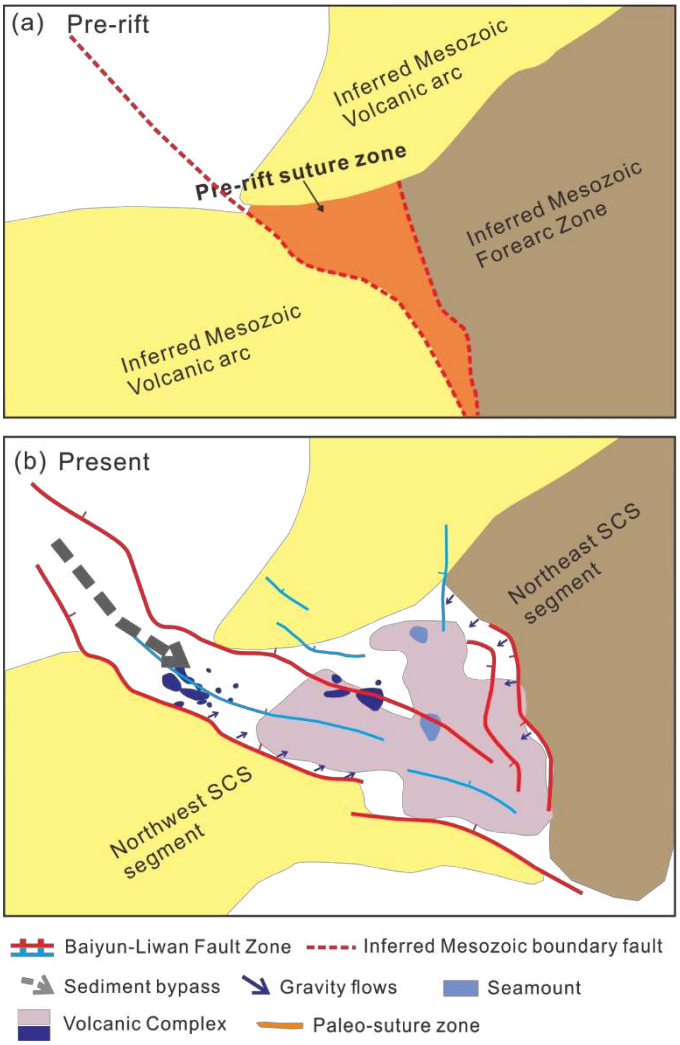

669

670 Fig. 9. Evolution of the BLFZ across the northern South China Sea. The BLFZ coincides with a basement fault

671 zone following the boundary between two distinct terranes. Its strike has later influenced the orientation of

672 Cenozoic extensional faults, giving rise to a dominant NW–SE direction. Extreme crustal thinning and widespread

673 magmatism occurred along the BLFZ during the Cenozoic.

674 Table 1

675 Internal character of the three seismic sedimentary units interpreted in the BLFZ (Units 1 to 3).

Acoustic unit	Reflection characteristics			Key lithologies	Depositional setting	Age	Thickness TWT(s)
	Top	Bottom	Internal				
Unit 1	**T_7**: continuous, low- to moderate-amplitude	**T_8**: continuous, moderate- to high-amplitude	Chaotic reflections, variable amplitude	Sandstones, shales with thin-bedded siltstones	Fluvial-lacustrine	Paleocene-Early Oligocene	~0 - 3.08
Unit 2	**T_4**: continuous, moderate- to high-amplitude	**T_7**	Parallel to sub-parallel, low to moderate amplitude	Sandstones with shales, volcanics and limestones	deltaic to marginal marine, shallow marine	Late Oligocene-Early Miocene	~0.29 - 4.75
Unit 2A	**T_6**: relatively continuous, low- to moderate-amplitude **T_4**	**T_7**				Late Oligocene-Early Miocene	
Unit 2B		**T_6**				Early Miocene	
Unit 3	**Sea floor**: smooth, continuous wavy	**T_4**	Parallel, continuous, low to moderate amplitude	Claystones, siltstones with sandstones	deep-marine	Middle Miocene-Quaternary	~0 - 2.93

676

677